*metals*

MDPI

*Article*

# Investigation on the Dynamic Behaviors of Aluminum Foam Sandwich Beams Subjected to Repeated Low-Velocity Impacts

**Kailing Guo [1,2,*], Mengying Mu [2] and Shuo Zhou [2]**

[1] Key Laboratory of High Performance Ship Technology, Wuhan University of Technology, Ministry of Education, Wuhan 430063, China
[2] School of Naval Architecture, Ocean and Energy Power Engineering, Wuhan University of Technology, Wuhan 430063, China; mumengying30@163.com (M.M.)
* Correspondence: guokailing@whut.edu.cn; Tel.: +86-1507-247-7235

**Abstract:** Marine structures are frequently subjected to repeated-impact loadings during navigation and operation. The structural damage accumulates, resulting in structural failures and even serious accidents. Experiments were performed using an INSTRON drop tower to investigate the dynamic behaviors of aluminum foam sandwich beams (AFSBs) subjected to repeated impacts; moreover, the mechanism of plastic deformation and damage and the energy absorption characteristics were analyzed. The results showed that as the number of impacts increased, the AFSB experienced progressive failure. The peak impact force, the deflection of the face sheets, and the rebound velocity gradually increased with increasing numbers of impacts, while their increments declined. However, when cracks occurred on the aluminum foam core and face sheets, as the number of impacts increased, the peak force and the rebound velocity decreased, while the amount of deflection in the front and back faces progressively increased. Before the foam core cracked, as the number of impacts increased, the elastic energy increased, while the plastic energy decreased. Once the foam core cracked, the plastic energy increased suddenly. During repeated impacts, the energy absorbed via local indentation in each impact initially increased with the number of impacts, and then decreased before finally becoming constant.

**Keywords:** aluminum foam sandwich beam; dynamic behavior; local indentation; experiments; repeated impacts

check for updates

**Citation:** Guo, K.; Mu, M.; Zhou, S. Investigation on the Dynamic Behaviors of Aluminum Foam Sandwich Beams Subjected to Repeated Low-Velocity Impacts. *Metals* **2023**, *13*, 1115. https://doi.org/10.3390/met13061115

Academic Editor: Matej Vesenjak

Received: 15 May 2023
Revised: 2 June 2023
Accepted: 6 June 2023
Published: 13 June 2023

**Copyright:** © 2023 by the authors. Licensee MDPI, Basel, Switzerland. This article is an open access article distributed under the terms and conditions of the Creative Commons Attribution (CC BY) license (https://creativecommons.org/licenses/by/4.0/).

## 1. Introduction

Marine structures are frequently exposed to repeated-impact loadings, such as collisions with supplying ships, dropped objects, and floe ice. During navigation and operation, structural damage accumulates, resulting in structural failure and even serious accidents. Therefore, studying the dynamic behaviors of engineering structures during repeated dynamic loadings is of practical engineering importance.

The dynamic behaviors of marine structures under the influence of repeated impacts has attracted increasing interest.

In 1990, Zhu studied the phenomenon of marine structures experiencing repeated collisions, and investigated the dynamic plastic responses of ship plating that was subjected to repeated impacts via experiments, a theoretical analysis, and numerical simulations [1]. A program based on the finite difference method was developed and an expression for the permanent deflection of the ship plate was derived. To further study the dynamic behavior of ship plating subjected to repeated impacts, Zhu and Faulkner [2] performed repeated-impact tests on fully clamped rectangular plates with a rigid wedge striker, and obtained a correlation between permanent deflection and the number of impacts. Afterward, Zhu et al. [3] carried out experimental and theoretical studies on the dynamic responses of a stiffened ship plate to repeated impacts, and the plastic responses of the

stiffened plate were analyzed. Recently, He and Saroes [4–7] performed experimental studies and numerical investigations on a beam and plate that was exposed to repeated low-velocity impacts, and the relationship between the dynamic responses and the number of impacts was examined. Additionally, the phenomenon of pseudo-shakedown was discussed. Truong et al. [8] employed numerical simulations to examine the effect of impact location on the dynamic behavior of a steel plate exposed to repeated low-velocity impacts.

Metal foam is a type of lightweight material that has a high specific strength, high specific stiffness, and excellent energy absorption capacity. It has been widely used in the industry [9–11]. Over the last two decades, due to the rapid development of methods for manufacturing metal foam materials [12–14], their wide applications in the field of engineering, and their excellent mechanical properties, the dynamic behaviors of metal foam materials have attracted extensive attention. Rajak et al. [15] experimentally investigated the effects of density and a high strain rate on the crushing responses of composite metallic foams (CMFs). The results showed that the factor contributing the most was the strain rate, followed by the relative density and then the microstructure. Linul et al. [16] conducted quasi-static compression tests and impact tests on CMFs under different temperatures to analyze the crashworthiness of lightweight CMFs at high temperatures. The results showed that the lightweight CMFs had a strongly temperature-dependent deformation behavior, and transitioned from brittle to ductile with increasing testing temperature.

As foam core sandwich structures have excellent impact resistance and energy absorption, they have been widely used in engineering applications [17–21]. An increasing number of researchers have begun to investigate the mechanical behaviors of metal foam core sandwich structures subjected to impact loadings.

Yu et al. [22,23] conducted quasi-static and dynamic three-point bending tests to determine the dynamic responses and failure modes of an aluminum foam sandwich beam (AFSB). The results showed that when the thickness of the face sheet was smaller, the front face wrinkled while the back face mainly experienced stretching failure. The failure modes of the AFSB mainly included local indentation, core shear, and face sheet yield. To further investigate the failure mechanism of AFSB, Crupi and Montanini [24] performed dynamic three-point bending tests and found that the span length affected the failure modes of the AFSB significantly. Jing et al. [25–27] studied the dynamic responses of an AFSB exposed to impulsive loadings. In these studies, the deformation process was recorded using a high-speed camera system and the dynamic responses and failure modes of the AFSB were discussed. Meanwhile, the influence of the face and core thicknesses on the dynamic behavior of the AFSB was examined. Tan et al. [28] investigated the dynamic responses of AFSBs that were subjected to rigid mass impacts, analyzing the mechanical mechanism and failure modes. The results showed that when the core thickness was small, the failure mode involved stretching due to overall bending. However, when the core thickness was large, the main failure modes were overall bending and core shearing. In order to improve the impact resistance of AFSBs via structural optimization, the mechanical properties of gradient metal foam sandwich structures have been investigated. Jing et al. [29] carried out impact tests on metal foam gradient sandwich beams. Additionally, some researchers performed numerical and theoretical analyses to determine the dynamic behaviors of gradient metal foam sandwich beams (MFSBs) under single-impact loadings [30–32]. Zhou et al. [33] established an analytical model of fully clamped sandwich beams with layered gradient foam cores under low-velocity impacts, and the interactions between bending and stretching were taken into account.

Recently, the dynamic behavior of sandwich structures under repeated impacts has attracted increasing attention. Zhu et al. [34] carried out numerical studies on aluminum foam sandwich beams under repeated low-velocity impacts and analyzed their dynamic behavior and energy absorption. Zeng et al. [35] investigated the dynamic behavior of aluminum corrugated core sandwich structures subjected to repeated impacts. The results showed that the dynamic responses of sandwich structures under repeated impacts were

vastly different from those of sandwich structures subjected to a single impact, especially in terms of deformation performance and energy consumption.

Numerous investigations have been published on the dynamic behaviors of AFSBs, specifically their deformation and failure modes as well as their energy absorption, but few studies have been carried out on the dynamic behaviors of AFSBs subjected to repeated-impact loadings. When an AFSB is exposed to repeated-impact loadings, the impact energy accumulates with the increase in the number of impacts, and the deformation and failure modes, the loading and unloading stiffnesses, and the energy absorption performance are considerably different from those of an AFSB exposed to a single impact. The mechanism of deformation and damage accumulation as well as the energy absorption characteristics have not been identified. Thus, it is necessary to investigate the dynamic behaviors of AFSBs subjected to repeated impacts.

Metal foam contains many kinds of materials that have similar physical and mechanical properties, such as its low relative density, large porosity (50–80%), high strength-to-weight ratio, high stiffness-to-weight ratio, and excellent energy absorption ability; aluminum foam is a typical representative of metal foam.

This study conducted low-velocity impact tests on AFSBs to reveal the mechanism of deformation and damage accumulation, as well as their energy absorption characteristics when subjected to repeated impacts. In the repeated-impact tests, the deformation and failure modes of AFSBs were analyzed and the mechanism of deformation and damage accumulation was determined. Meanwhile, the correlation between the dynamic responses of AFSBs and the number of impacts was examined. In addition, the performance of AFSBs in terms of their energy absorption during overall bending and local indentation was analyzed. Experimental studies on the dynamic behavior of AFSBs exposed to repeated impacts can provide a reference for designing durable marine structures, which are often subjected to repeated-impact loadings.

## 2. Materials and Experiment Setup

### *2.1. Specimen and Material Properties*

The metal foam sandwich beam was composed of a front face sheet, a back face sheet, and an aluminum foam core. Epoxy resin was used to glue the face sheets and the core. The thicknesses of the face sheets and the core were $t$ = 1 mm and $c$ = 10 mm, respectively. The total length and the span length of the AFSB were $L_B$ = 250 mm and $L_S$ = 150 mm, respectively, and the width of the beam was $B$ = 30 mm. Thus, the ratio of length to width was $L_S/B$ = 5, and the ratio of length to thickness was $L_s/(c + 2t)$ = 12.5. Figure 1 displays the AFSB specimen and its dimensions.

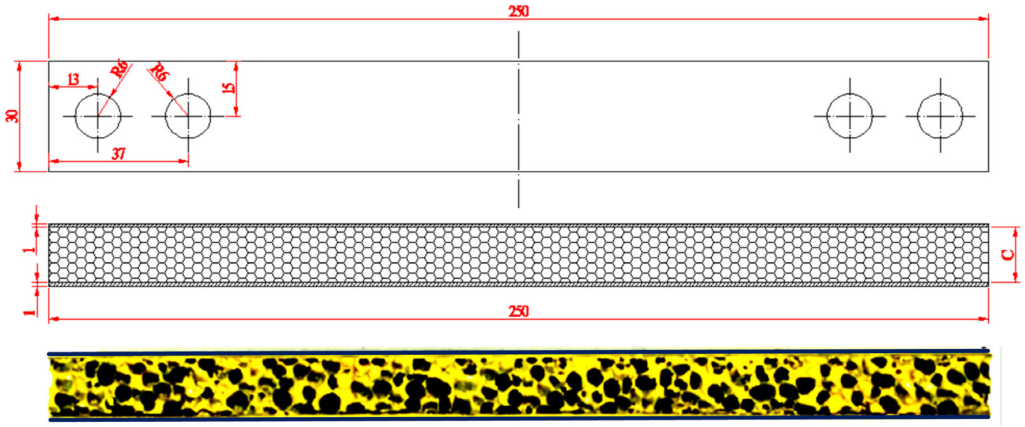



**Figure 1.** AFSB specimen.

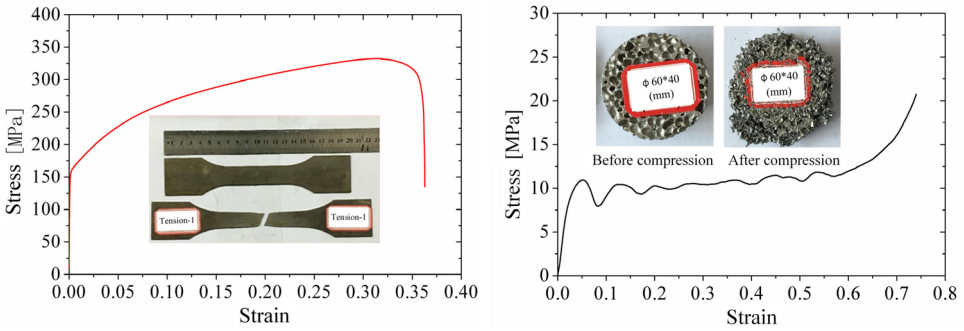
The material of the face sheets was mild steel. The core material was closed-cell aluminum foam with a density of 0.5 g/cm$^3$. Its relative density was 0.185, and the average

size of the cellular cores was 3 mm. The closed-cell aluminum foam was produced via a liquid route, and the fabrication method used was melt gas injection [9]. The steps for fabricating the metal foam were as follows:

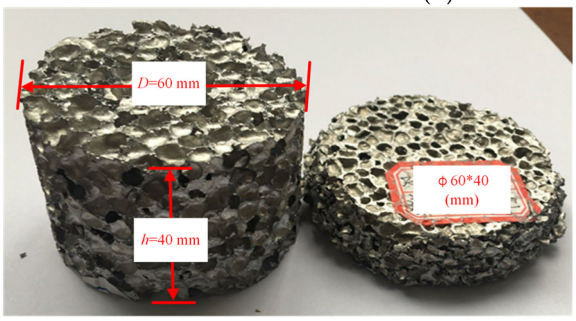
1. The melted aluminum was prepared and poured into a container.
2. Rotating impellers were used to create fine gas bubbles in the melted aluminum and distribute them uniformly.
3. The liquid metal was drained out, leaving behind a fairly dry liquid foam.
4. A conveyor belt was used to skim off the liquid foam from the liquid surface, and then the foam was allowed to cool down to a semisolid state.
5. The semisolid foam was flattened by means of top-mounted rolls to yield a foam slab with closed, well-distributed cores.

The aluminum foam specimens were cut from large blocks into cylinders that were 40 mm in height and 60 mm in diameter for the quasi-static uniaxial compression tests.

As shown in Figure 2, the engineering stress–strain curves of mild steel and aluminum foam were obtained from quasi-static tests. Tables 1 and 2 present the properties of mild steel and aluminum foam.




(**a**) Mild steel (**b**) Aluminum foam




(**c**) Macroscopic image of aluminum foam before and after tests

**Figure 2.** Engineering stress–strain curves and image of aluminum foam in compression test.

**Table 1.** Properties of mild steel.

| Density ($kg/m^3$) | Young's Modulus (GPa) | Poisson's Ratio | Yield Stress (MPa) |
|---|---|---|---|
| 7800 | 201 | 0.3 | 182 |

**Table 2.** Properties of aluminum foam.

| Density ($g/cm^3$) | Relative Density | Young's Modulus (GPa) | Plateau Stress (MPa) | Densification Strain |
|---|---|---|---|---|
| 0.5 | 0.185 | 0.42 | 10 | 0.6 |

### 2.2. Equipment for the Experiment

The impact tests were conducted using an INSTRON 9350 drop tower (ITW Ltd, Norwood, MA, USA) as depicted in Figure 3. The top of the additional mass frame was connected with a spring acceleration system, resulting in a maximum velocity of up to 24 m/s. Before the impact tests were conducted, the AFSB was clamped both ends with bolts to provide a fully clamped boundary condition, as illustrated in Figure 4. The impactor with a wedge nose (as presented in Figure 5) was connected with a force transducer, and the acquisition frequency used was 500 kHz. During the impact tests, all of the data were obtained from the force transducer via the data acquisition system (DAS 64 K). Thus, the time histories of velocity $v(t)$, displacement $D(t)$, and absorbed energy $E(t)$ could be converted from the time history of the impact force, as described in Equations (1)–(3).

$$v(t) = v_0 + \int_0^t \frac{F(t)}{M} dt \tag{1}$$

$$D(t) = \int_0^t v(t) dt \tag{2}$$

$$E(t) = \int_0^t F(t) dD(t) = \int_0^t F(t) v(t) dt \tag{3}$$

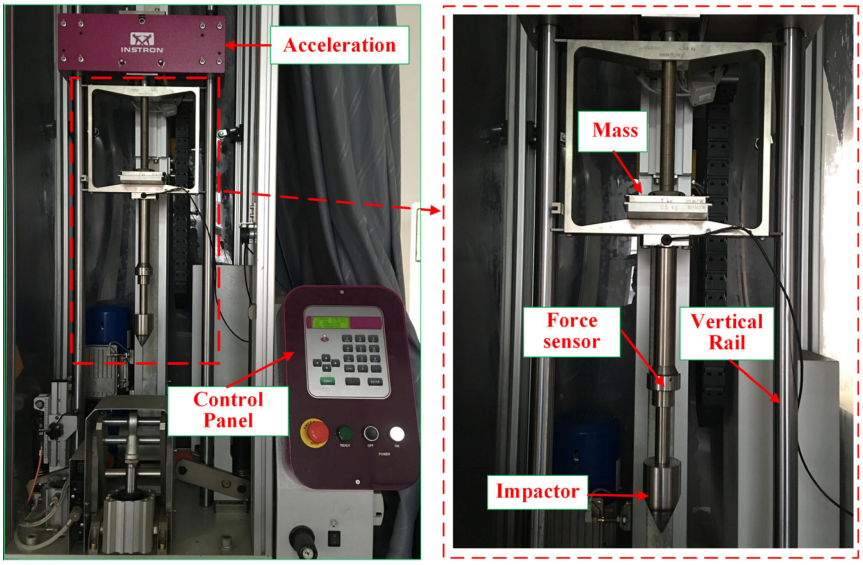



**Figure 3.** INSTRON 9350 drop tower.

In this research, four cases were studied, as displayed in Table 3. Three specimens with the same structural configuration were provided for each case, in order to reduce experimental error. The impactor mass was 7.884 kg, while for each of the four cases, the impact energy was changed by setting the initial impact velocity.

**Table 3.** Parameters of the different cases.

| Case | Energy (J) | Mass (kg) | Velocity (m/s) | Core Thickness (mm) | Face Thickness (mm) |
|---|---|---|---|---|---|
| BE1 | 7.746 | 7.884 | 1.40 | 10 | 1.0 |
| BE2 | 17.750 | 7.884 | 2.12 | 10 | 1.0 |
| BE3 | 27.800 | 7.884 | 2.66 | 10 | 1.0 |
| BE4 | 37.800 | 7.884 | 3.10 | 10 | 1.0 |

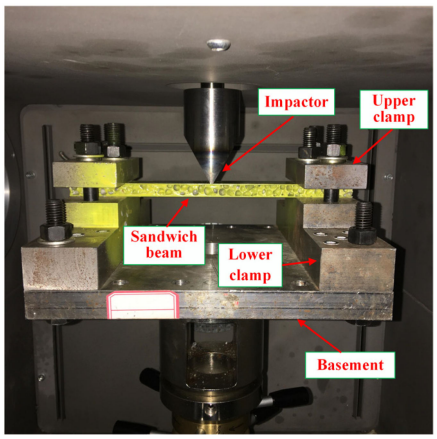



**Figure 4.** Clamp and basement.

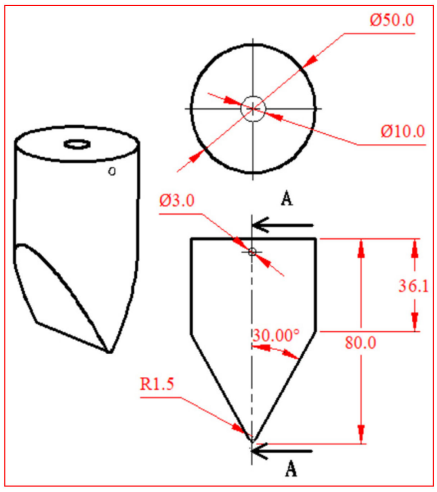



**Figure 5.** Dimensions of the impactor.

## 3. Dynamic Behaviors of AFSBs subjected to Repeated Impacts

### *3.1. Deformation and Failure*

#### 3.1.1. Boundary Condition

In the experiment, bolts were used to constrain the ends of the sandwich beam. However, in a real situation, due to boundary conditions, it is difficult to fully clamp a beam, and its ends may slip to some extent.

Figure 6 shows an example of boundary slipping of the AFSB for case BE3. It is clear that the boundary slipping was quite small after the first six impacts. On the 9th impact, the boundary slipping became comparably larger but the value was still small. The boundary slipping increased with the number of impacts. However, compared with the axial elongation, the value of boundary slipping was relatively small, and could be neglected in the analysis. Therefore, in this study, the boundary condition was assumed to be a fully clamped beam.

#### 3.1.2. Deformation and Failure Modes

Compared with the aluminum foam core, the face sheet was relatively stronger. Therefore, the foam core was easily compressed along the direction of the thickness. To explain the deformation pattern of the AFSB, the loading state of the AFSB subjected to a wedge mass impact is presented in Figure 7. Under a wedge mass impact, the front face is subjected to a concentrated force from the impactor and the loading area is adjacent to the middle span of the beam. Owing to the concentrated force, the front face sheet will bend, resulting in the overall compression of the foam core. Accordingly, the foam core provides

support to the front face and compression to the back face. Therefore, the front face sheet is subjected to concentrated force and distributed pressure, the back face sheet is mainly subjected to distributed pressure, while the foam core experiences distributed pressure from the front and back face sheets.

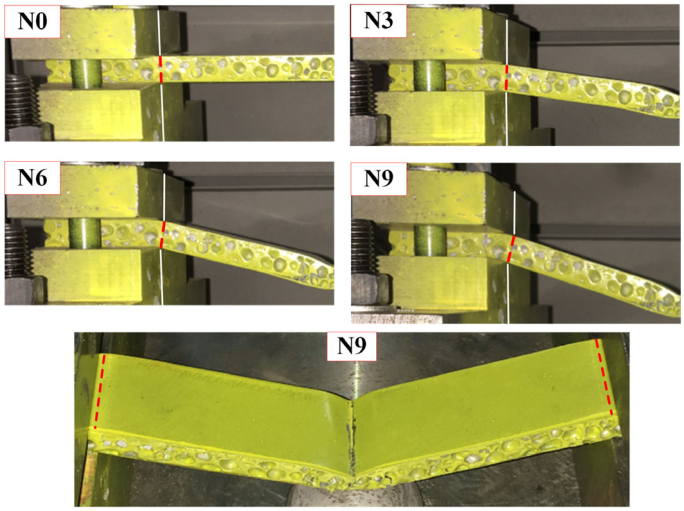



**Figure 6.** Boundary slipping of an AFSB after different numbers of impacts.

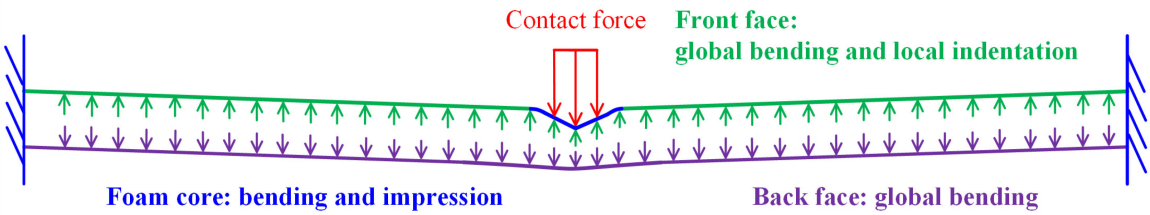



**Figure 7.** Loading state of an AFSB subjected to a wedge mass impact.

As discussed above, the loading state of the sandwich beam was decides by its deformation pattern. When subjected to impact loadings, the AFSB not only experienced global bending but also local indentation, as presented in Figure 8. In addition, the front face sheet underwent global bending and local indentation. In our experiment, two plastic hinges adjacent to the indentation were observed. Meanwhile, the back face sheet experienced global bending, while the foam core presented global bending and compression accompanied by local indentation. In addition, plastic hinges occurred at the middle span and the boundary and the displacement was almost linearly distributed from the middle span to the clamped boundary.

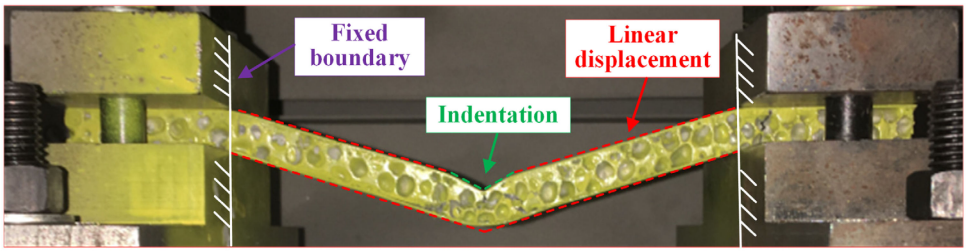



**Figure 8.** Deformation mode of an AFSB.

As for case BE1 (E = 7.746 J) and case BE2 (E = 17.75 J), their initial impact energy was less than 20 J; the impact test was repeated 10 times, and neither the face sheet nor the foam core experienced fracture on the 10th impact. The overall bending and local indentation of the AFSB increased with the number of impacts, due to the energy accumulated during

the repeated impacts, as shown in Figure 9a,b. As for the overall deformation of the AFSB, the deformation profile exhibited excellent symmetry, the distribution of the displacement was approximately linear, and the plastic hinges were located at the middle span and the clamped boundary. With the increase in the number of impacts, small cracks began to appear at the plastic hinges of the sandwich beam and progressive failure occurred.

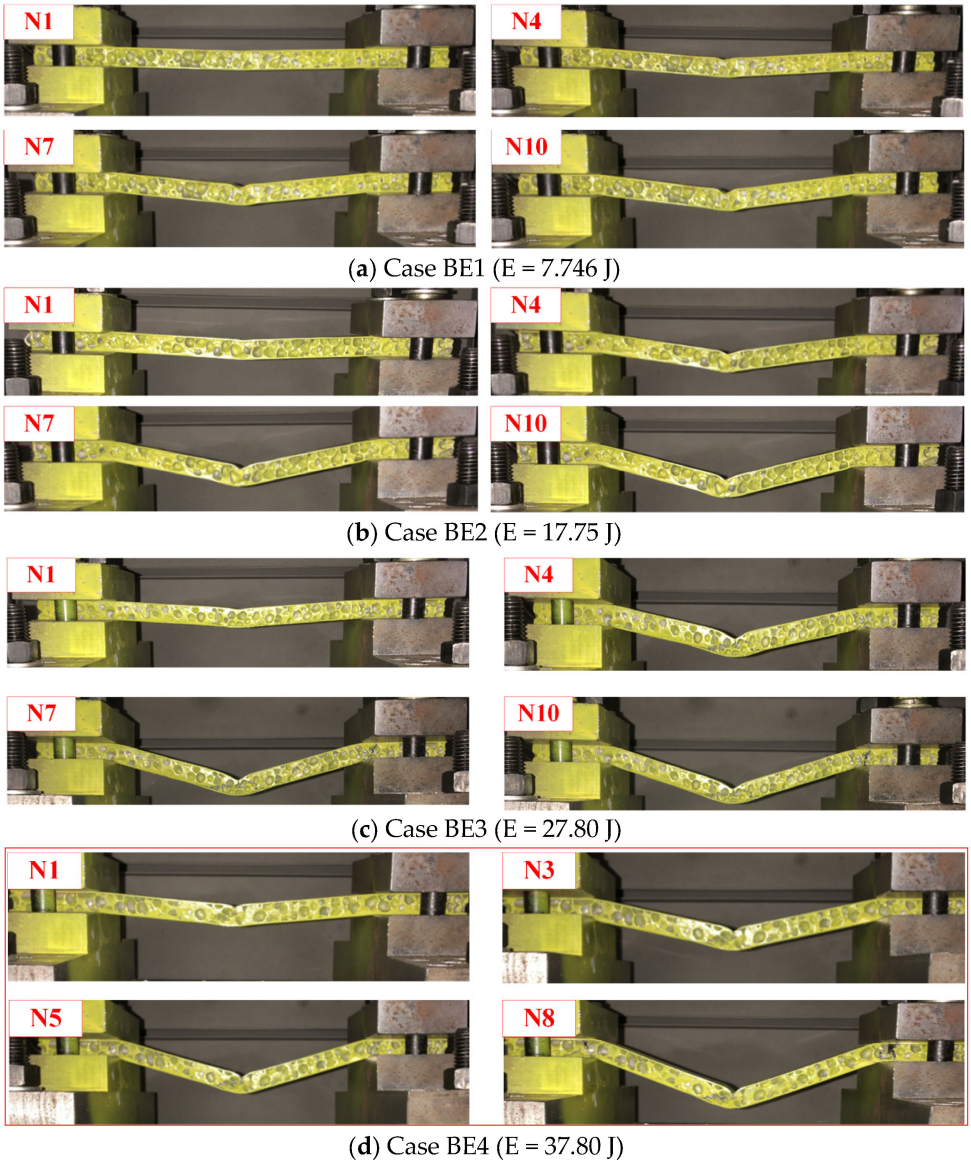



**Figure 9.** Deformation profiles of AFSBs during repeated-impact tests.

As for the groups with a larger impact energy, such as case BE3 (E = 27.80 J), the 7th impact led to a crack on the core. For case BE4 (E = 37.80 J), a crack occurred on the core on the 5th impact. As displayed in Figure 9c,d, the AFSB elongated, and the angle of the plastic hinge increased gradually with an increase in the number of impacts. When the amount of energy absorbed by the AFSB reached a certain value, a crack began to form at the middle span and the two ends and expanded gradually with the number of impacts. Meanwhile, due to the large deflection of the AFSB, delamination between the face sheet and the foam core appeared adjacent to the impact location and the boundary. At this moment, the loading capacity of the AFSB declined rapidly.

When the number of impacts reached a certain value, the AFSB failed, as shown in Figure 10. When sandwich beams are subjected to repeated impacts, several deformation

modes can be observed, such as large inelastic deformation, core compression, and core shear with interfacial failure. As for the front and back face sheets, longitudinal stretching and plastic hinges at the boundary and middle span due to large plastic deformation are the main failure modes. However, no face wrinkling mode was observed in the impact tests, which is different from the phenomenon that occurred on a sandwich beam with a thin face and a strong core used in reference [25]. In contrast, the foam core failure mode was dominated by core compression, core tensile fracture, and core shear accompanied by interfacial delamination. As the sandwich beam underwent bending deformation, the foam core experienced global bending and longitudinal stretching, leading to tensile fracture at the support and the middle span. Since the strength of the adhesive layer was lower than that of the core shear strength, when large plastic deformation occurred, delamination appeared between the face sheet and the foam core.

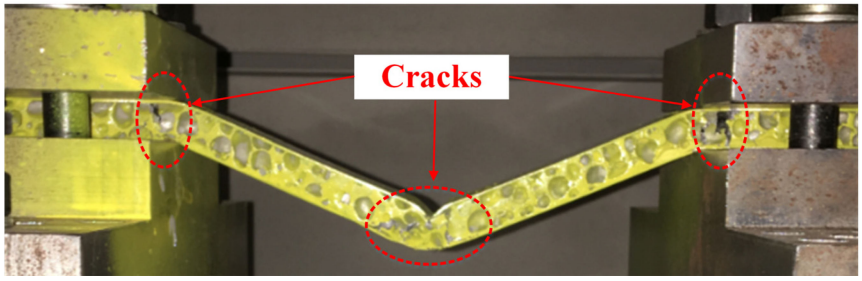



**Figure 10.** Failure mode of the AFSB.

When an AFSB is subjected to repeated impacts, the energy it absorbs accumulates with the number of impacts, resulting in the accumulation of plastic deformation. The deformation patterns and the failure modes of AFSBs change as the number of impacts increases, leading to progressive failure.

### *3.2. Dynamic Responses of AFSBs*

In contrast with what happens during a single impact, when an AFSB experiences repeated impacts, the deformation and damage accumulate. According to whether cracks appeared on the metal foam, the results of the impact tests were divided into two groups: group A (case BE1 and case BE2) and group B (case BE3 and case BE4). In group A, no failure was observed, while in group B, the front face sheet and the foam core fractured. To better understand the dynamic behavior of the AFSB, the characteristics of the impact force, the rebound velocity, the absorbed energy, the impact force vs. displacement, and the deflection vs. the impact number are examined.

#### 3.2.1. Impact Force

Figure 11 displays the time history curves of the impact force. A force platform appeared in all instances (irrespective of the number of impacts) due to the compression of the aluminum foam core during impact. As for case BE1 and case BE2, the peak value of the impact force increased with an increase in the number of impacts. For case BE3 and case BE4, the metal foam core cracked on the 7th impact and the 5th impact, respectively, as shown in Figure 9; as a result of the cracked core, the loading capacity of the AFSB decreased rapidly. Therefore, after a certain number of impacts, the AFSB cracked, and the peak value of the impact force began to decline.

As for Case BE4, after the 8th impact, a longitudinal fracture appeared on the metal foam core, as it no longer had the capacity to resist axial stretching. At this moment, the front face experienced bending and stretching and the foam core was compressed, leading to the second platform of impact force, as demonstrated in Figure 11d.

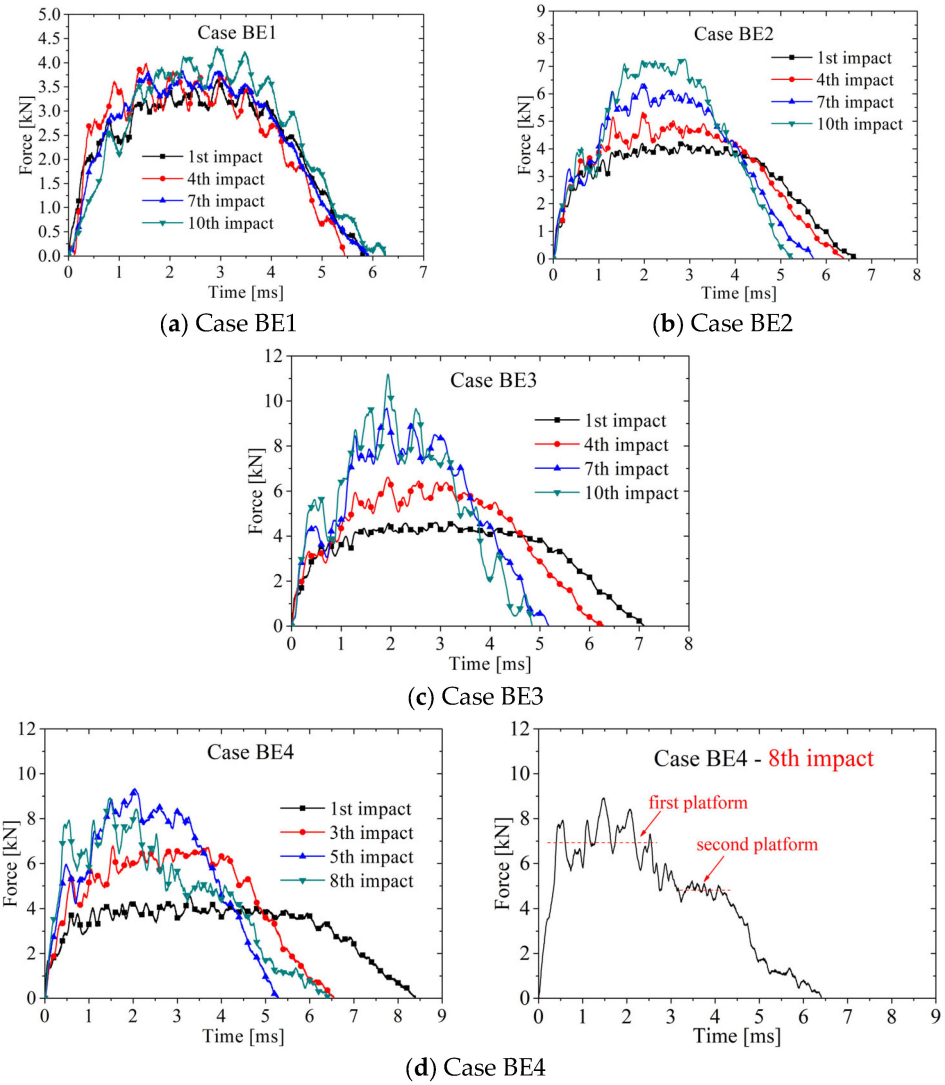



**Figure 11.** Time history curves of impact force.

### 3.2.2. Rebound Velocity

As presented in Figure 12, the impact velocity decreased with an increase in the impact time. Once its value declined to zero, the impact velocity increased in the opposite direction until the impactor separated from the surface of the AFSB. The velocity at the moment that the impactor separates from the surface of the AFSB is defined as the rebound velocity. When the impact velocity reduces to zero, all of the initial kinetic energy of the impactor has been transformed into strain energy, including elastic deformation energy and plastic deformation energy. The elastic deformation can be released in the form of the rebound kinetic energy of the impactor.

In case BE1 and case BE2, the rebound velocity increased with an increase in the number of impacts, as shown in Figure 12a,b. However, when the metal foam core experienced fracture, the rebound velocity decreased, as shown in Figure 12c,d, and the corresponding cases were the 10th impact for case BE3, and the 8th impact for case BE4.

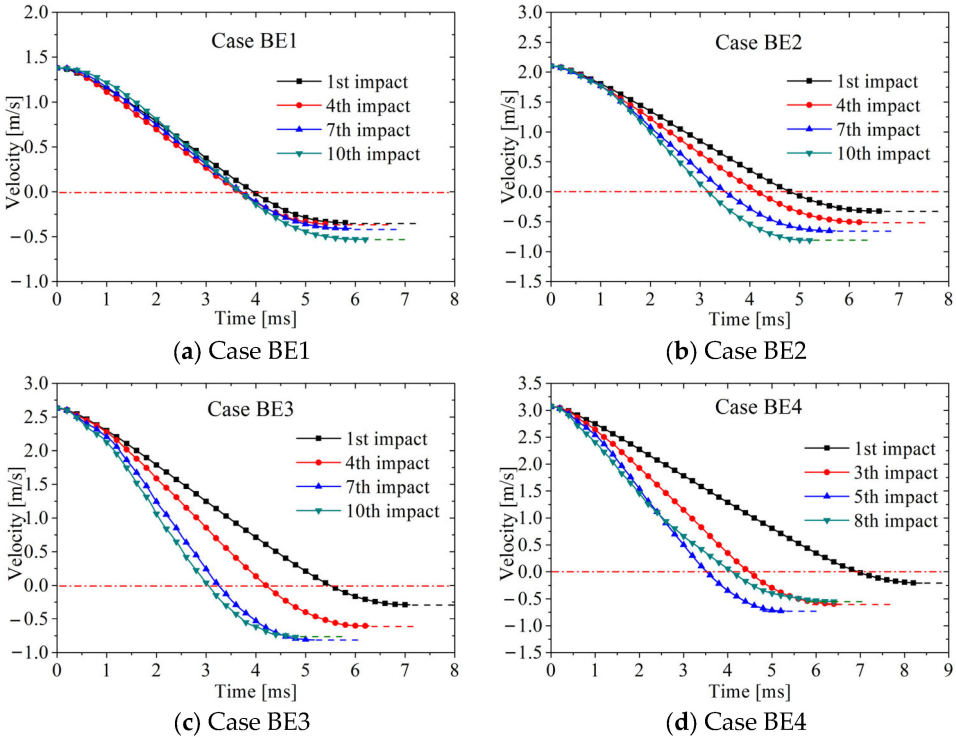



**Figure 12.** Time history curves of impact velocity.

### 3.2.3. Absorbed Energy

Figure 13 shows the time history curves of energy absorption by the AFSB. As the impact time increased, the absorbed energy initially increased, and then decreased to a certain value. When the velocity of the impactor decreased to zero, the deformation of the AFSB reached its maximum value and all of the kinetic energy was transformed into the deformation energy of the AFSB. Then, the elastic energy stored in the AFSB began to be released and the energy absorbed by the AFSB decreased until the face sheet and the impactor separated.

As shown in Figure 9, as the number of impacts increased, the deformation of the AFSB gradually increased, which included transverse bending and longitudinal stretching. An increase in longitudinal stretching can lead to an increase in the membrane force, resulting in an increase in the elastic deformation energy. Hence, with an increase in the number of impacts, the elastic deformation energy of the AFSB increased, while the permanent energy absorption decreased, as presented in Figure 13a,b. However, when the foam core fractured, the energy consumed due to plastic deformation increased and the elastic deformation energy decreased, as presented in Figure 13c,d.

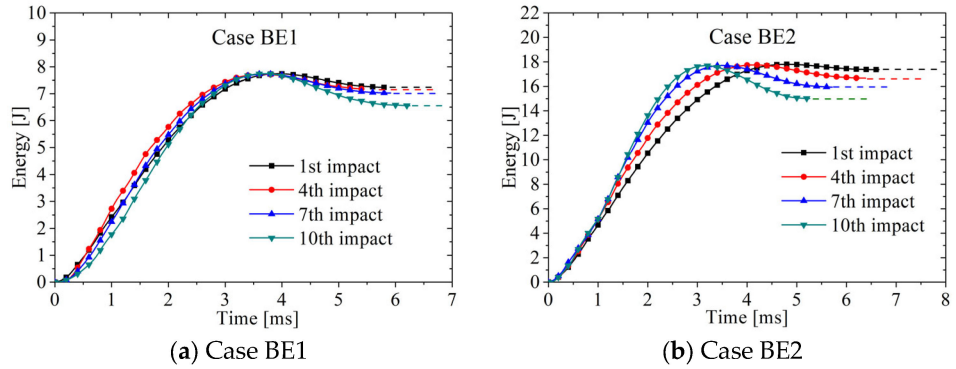
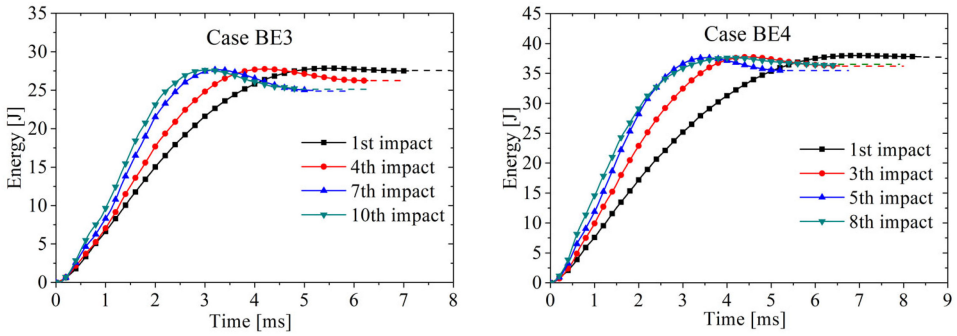



**Figure 13.** *Cont.*



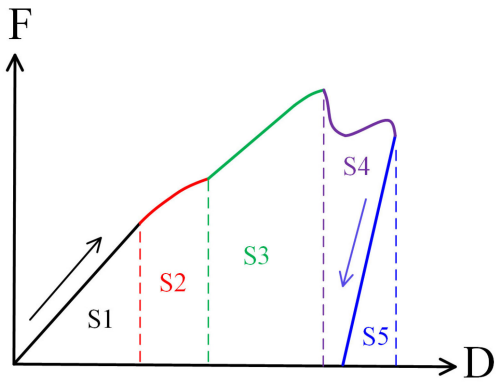

(**c**) Case BE3 (**d**) Case BE4

**Figure 13.** Time history curves of energy absorption.

### 3.2.4. Impact Force vs. Displacement

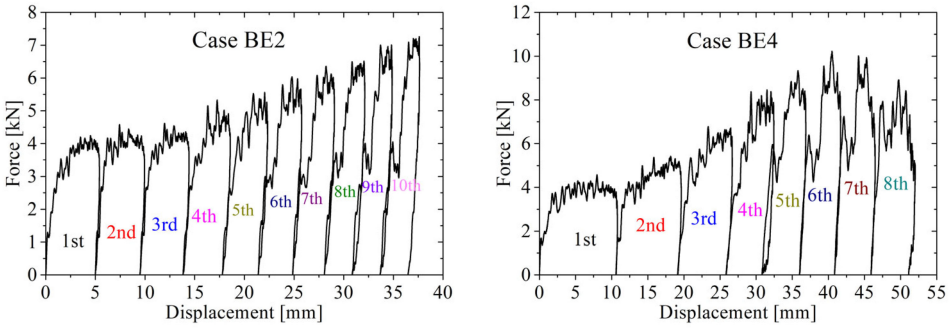
A force vs. displacement curve can not only reflect the loading and unloading process, it can also illustrate characteristics of the energy absorption.

As shown in Figure 14a, according to the characteristics of loading and unloading, the force–displacement curve was divided into five stages, from S1 to S5. In the first stage (S1), the AFSB exhibited global elastic bending and the impact force increased almost linearly with the displacement. In the second stage (S2), plastic deformation occurred, and the slope of the force–displacement curve decreased. The front face sheet experienced overall bending accompanied by local indentation, while the metal foam core was compressed adjacent to the impact location. As the displacement increased, the depth and width of the indentation enlarged, while the metal foam compressed to a value where the local indentation would no longer increase. In the third stage (S3), the AFSB mainly experienced overall bending, and the bending stiffness of the AFSB increased, i.e., the slope of the force–displacement curve increased. In the fourth stage (S4), as the number of impacts increased, failure occurred on the front face sheet and the foam core due to large axial stretching, leading to a decline in the impact force. Then, the foam core adjacent to the impact area was compressed to a state of densification. Finally, the back face experienced axial stretching, and the impact force increased. When the total kinetic energy of the impactor was absorbed by the AFSB, the displacement no longer increased, leading to the fifth stage (S5). In this stage, the elastic energy was released and the impactor rebounded. the elastic unloading stiffness under the previous impact was almost equal to the loading stiffness under the next impact, and the loading stiffness increased with the number of impacts, as illustrated in Figure 14b,c.




(**a**) Simplified illustration of the loading and unloading process

**Figure 14.** *Cont.*




(**b**) Case BE2 (**c**) Case BE4

**Figure 14.** Force–displacement curve of AFSBs under repeated impacts.

As for a lower impact energy, such as in cases BE1 and BE2, no fracture was observed on the front face sheet and the foam core, leading to the elimination of stage 4 (S4), as plotted in Figure 14b. In contrast, for higher impact energy, such as in cases BE3 and BE4, the front face sheet and the foam core experienced fracture, leading to the occurrence of all five stages, as presented in Figure 14c.

### 3.2.5. Deflection vs. Impact Number

To investigate the dynamic responses of AFSBs under repeated impacts, the correlations between front and back face deflections, core compression, and impact number were analyzed. The detailed data are presented in Tables 4 and 5.

**Table 4.** Deflections of AFSBs for case BE1 and case BE2 (unit: mm).

| | Case BE1 | | | Case BE2 | | |
|---|---|---|---|---|---|---|
| **Impact Number** | **Front Face** | **Back Face** | **Foam Core** | **Front Face** | **Back Face** | **Foam Core** |
| 1 | 1.70 | 1.54 | 0.16 | 3.85 | 3.59 | 0.26 |
| 2 | 3.31 | 2.95 | 0.36 | 6.86 | 6.16 | 0.70 |
| 3 | 4.60 | 4.01 | 0.59 | 9.46 | 8.49 | 0.97 |
| 4 | 5.77 | 4.92 | 0.85 | 11.78 | 10.63 | 1.15 |
| 5 | 6.87 | 5.76 | 1.11 | 13.85 | 12.56 | 1.29 |
| 6 | 7.85 | 6.50 | 1.35 | 15.61 | 14.19 | 1.42 |
| 7 | 8.80 | 7.27 | 1.53 | 17.04 | 15.49 | 1.55 |
| 8 | 9.62 | 7.99 | 1.63 | 18.35 | 16.69 | 1.66 |
| 9 | 10.40 | 8.67 | 1.73 | 19.30 | 17.56 | 1.74 |
| 10 | 10.93 | 9.16 | 1.77 | 20.05 | 18.23 | 1.82 |

**Table 5.** Deflections of AFSBs for case BE3 and case BE4 (unit: mm).

| | Case BE3 | | | Case BE4 | | |
|---|---|---|---|---|---|---|
| **Impact Number** | **Front Face** | **Back Face** | **Foam Core** | **Front Face** | **Back Face** | **Foam Core** |
| 1 | 5.45 | 5.03 | 0.42 | 7.95 | 6.85 | 1.10 |
| 2 | 10.15 | 8.90 | 1.25 | 13.90 | 12.39 | 1.51 |
| 3 | 14.16 | 12.38 | 1.78 | 17.84 | 16.12 | 1.72 |
| 4 | 17.09 | 15.07 | 2.02 | 20.90 | 19.09 | 1.81 |
| 5 | 19.15 | 17.03 | 2.12 | 23.15 | 21.25 | 1.90 |
| 6 | 20.95 | 18.76 | 2.19 | 25.63 | 23.65 | 1.98 |
| 7 | 22.36 | 20.14 | 2.22 | 28.15 | 26.04 | 2.11 |
| 8 | 23.98 | 21.73 | 2.25 | 31.46 | 29.12 | 2.34 |
| 9 | 25.40 | 23.13 | 2.27 | / | / | / |
| 10 | 26.83 | 24.53 | 2.30 | / | / | / |

As for repeated impacts, the impact energy accumulated with increasing numbers. As seen from Figure 15, as the number of impacts increased, the permanent deflections of the face sheets increased, while the increments declined. When the metal foam core

fractured, the carrying capacity of the AFSB decreased suddenly, resulting in an increase in the amount of face sheet deflection.

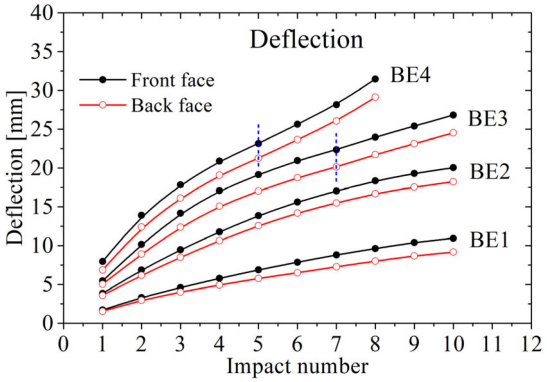



**Figure 15.** Permanent deflection vs. impact number.

Taking case BE3 as an example, the curves of correlation between deflection and impact number can be fitted as follows:

$$D_f = -0.583 + 6.691N - 0.696N^2 + 0.03N^3 \quad (4)$$

$$D_b = 0.01 + 5.476N - 0.524N^2 + 0.022N^3 \quad (5)$$

During repeated impacts, the AFSB displayed global bending and local indentation. The permanent deflection of the front face is the sum of global bending and local indentation, and the deflection of the back face is equal to the amount of the global bending. Therefore, the difference in the deflections between the front face and the back face can be defined as the amount of local indentation, as expressed in Equation (6).

$$w_0 = W_T - W_b \quad (6)$$

$W_T$ represents the permanent deflection of the front face sheet, $W_b$ represents the permanent deflection of the back face sheet, and $w_0$ represents the amount of local indentation.

Combining Equations (4) and (5), the expression of local indentation can be fitted as follows:

$$w_0 = -0.593 + 1.215N - 0.172N^2 + 0.008N^3 \quad (7)$$

### *3.3. Analysis of Energy Absorption*

When the energy consumed due to friction is not considered, the energy consumed by the AFSB can be divided into two main parts: plastic deformation energy and elastic deformation energy. The elastic deformation energy is released and transformed into the kinetic energy of the impactor through its rebound velocity. The ratio of the absorbed energy to the initial kinetic energy is defined as the "energy absorption efficient" ($E_e$), and the ratio of the rebound energy to the initial kinetic energy is defined as the "rebound efficient" ($R_e$).

$$E_e = \frac{E_{\text{absorption}}}{E_{\text{impact}}} \quad (8)$$

$$R_e = \frac{E_{\text{rebound}}}{E_{\text{impact}}} \quad (9)$$

Table 6 presents the data relevant to energy absorption. As shown in Figure 16, the energy absorption coefficient decreased with the number of impacts, while after the core fractured, the energy absorption coefficient began to increase. The correlation between the energy absorption efficient and the impact number was fitted linearly. As for case BE1 and case BE2, the metal foam core did not fracture, even on the 10th impact. Therefore,

only one curve could be used to describe its characteristic energy absorption, as described in Equations (10) and (11). However, for case BE3 and case BE4, due to the fracture of the metal foam core, the curve had to be divided into two parts, which could be fitted as Equations (12) and (13).

$$E_{e1} = 0.956 - 0.007N \tag{10}$$

$$E_{e2} = 0.997 - 0.014N \tag{11}$$

$$E_{e3} = \begin{cases} 1.006 - 0.0154N & (0 \le N \le 7) \\ 0.882 + 0.003N & (N \ge 7) \end{cases} \tag{12}$$

$$E_{e4} = \begin{cases} 1.0098 - 0.015N & (0 \le N \le 5) \\ 0.898 + 0.0093N & (N \ge 5) \end{cases} \tag{13}$$

**Table 6.** Energy absorption for different cases.

| | Case BE1 | | Case BE2 | | Case BE3 | | Case BE4 | |
|---|---|---|---|---|---|---|---|---|
| **Impact Number** | ***Ee*** | $R_c$ | ***Ee*** | $R_c$ | ***Ee*** | $R_c$ | ***Ee*** | $R_c$ |
| 1 | 0.940 | 0.060 | 0.977 | 0.023 | 0.988 | 0.012 | 0.996 | 0.004 |
| 2 | 0.934 | 0.066 | 0.970 | 0.030 | 0.981 | 0.019 | 0.984 | 0.016 |
| 3 | 0.931 | 0.069 | 0.962 | 0.038 | 0.960 | 0.040 | 0.962 | 0.038 |
| 4 | 0.935 | 0.065 | 0.942 | 0.058 | 0.949 | 0.052 | 0.931 | 0.069 |
| 5 | 0.915 | 0.085 | 0.921 | 0.079 | 0.915 | 0.085 | 0.945 | 0.055 |
| 6 | 0.917 | 0.083 | 0.916 | 0.084 | 0.911 | 0.089 | 0.948 | 0.052 |
| 7 | 0.916 | 0.084 | 0.905 | 0.095 | 0.906 | 0.094 | 0.971 | 0.029 |
| 8 | 0.903 | 0.097 | 0.881 | 0.119 | 0.908 | 0.092 | 0.968 | 0.032 |
| 9 | 0.888 | 0.112 | 0.872 | 0.128 | 0.914 | 0.086 | / | / |
| 10 | 0.853 | 0.147 | 0.854 | 0.146 | 0.916 | 0.084 | / | / |

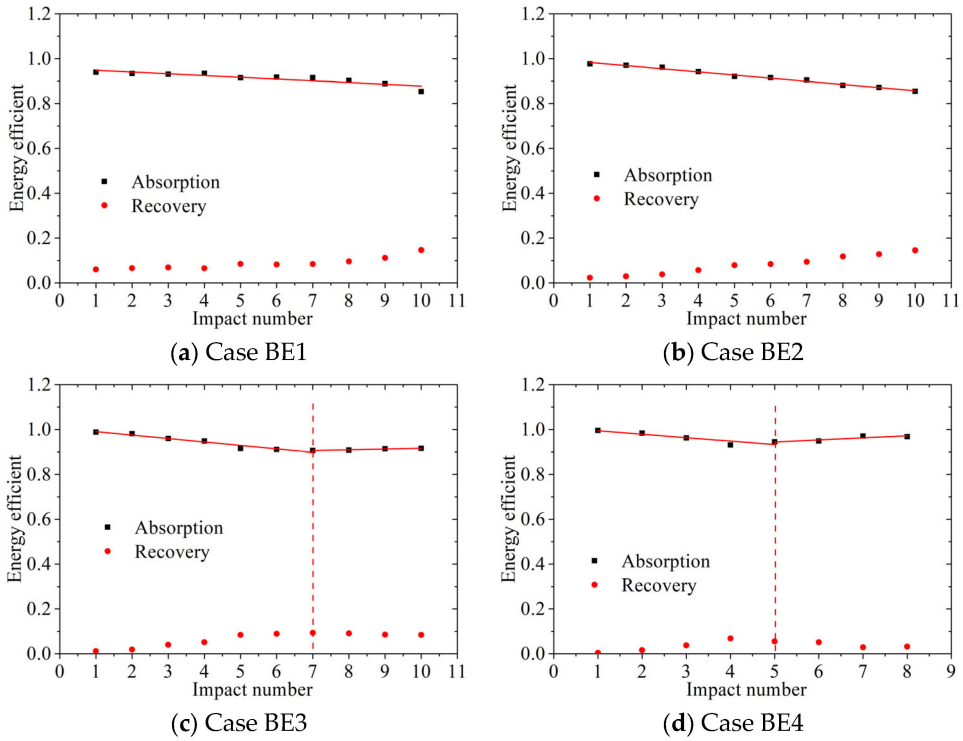



**Figure 16.** Correlation between energy absorption and impact number.

During repeated impacts, both global bending and local indentation consume energy and most of the kinetic energy of the impactor is transformed into plastic deformation energy. To identify the mechanism of energy absorption for overall bending and local indentation, a theoretical analysis can be applied to determine the relationship between the energy absorbed due to local indentation and the impact number. The energy consumed due to global bending can be obtained by the difference between the total energy absorbed and the energy absorbed due to local indentation.

The energy absorbed due local indentation can be predicted by theoretical analysis based on the rigid plastic foundation model [36,37]. Let us assume that the face sheet thickness is $t$, the width is $b$, the yield stress of the face sheet is $\sigma_f$, the platform stress of the aluminum foam core is $\sigma_c$, the local indentation is $w_0$, and the reaction force of indentation is $P$.

The initial collapse load is defined as follows:

$$P_i = 2b\sigma_c\lambda \tag{14}$$

where

$$\lambda = t \cdot \sqrt{\sigma_f \Big/ \sigma_c} \tag{15}$$

Then, we obtain the following:

$$\frac{P}{P_i} = \begin{cases} 1 + \frac{1}{2}\left(\frac{w_0}{t}\right)^2, & 0 \le \frac{w_0}{t} \le 1 \\ \frac{1}{2} + \frac{w_0}{t}, & \frac{w_0}{t} \ge 1 \end{cases} \tag{16}$$

The energy consumed due to local indentation can be expressed as the following:

$$U_i = \int_0^{w_f^*} P_i \cdot \frac{P(w_0)}{P_i} t \cdot dw_0^* \tag{17}$$

Then, we obtain the dimensionless expression as follows:

$$U_i^* = \frac{U_i}{P_i \cdot t} = \int_0^{w_f^*} \frac{P\left(w_0^*\right)}{P_i} \cdot dw_0^* \tag{18}$$

In combining Equations (14) and (18), we obtain the following:

$$U_i^* = \begin{cases} \frac{1}{6}\left(\frac{w_0}{t}\right)^3 + \frac{w_0}{t}, & 0 \le \frac{w_0}{t} \le 1 \\ \frac{1}{2}\left[\left(\frac{w_0}{t}\right)^2 + \frac{w_0}{t} + \frac{1}{3}\right], & \frac{w_0}{t} \ge 1 \end{cases} \tag{19}$$

The values of local indentation under different numbers of impact are provided via Equation (7). In combining Equations (14) and (19), the energy consumed due to local indentation can be obtained as follows:

$$U_i = U_i^* \cdot P_i \cdot t \tag{20}$$

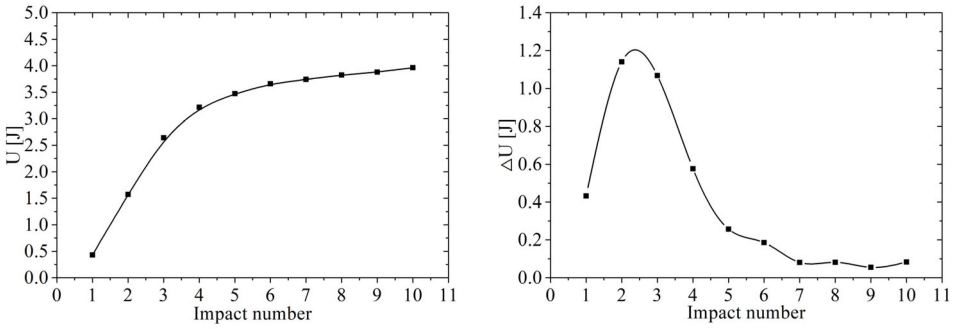
The plastic energy in terms of overall bending deformation is represented by the following:

$$U_b = U - U_i = U - U_i^* \cdot P_i \cdot t \tag{21}$$

Taking case BE3, for example, based on Equation (7) and Equations (14) to (21), the energy absorbed when local indentation ($U_i$) and overall bending ($U_b$) occur can be calculated. The relevant data are presented in Table 7 and plotted in Figures 17 and 18, respectively.

**Table 7.** Energy absorbed when local indentation occurs in case BE3.

| Impact Number | $w_0$ (mm) | $E_{absorbed}$ (J) | $U_b$ (J) | $U_i$ (J) | $\Delta U_i$ (J) |
|---|---|---|---|---|---|
| 1 | 0.42 | 27.518 | 27.086 | 0.432 | 0.432 |
| 2 | 1.25 | 27.308 | 25.735 | 1.573 | 1.141 |
| 3 | 1.78 | 26.689 | 24.048 | 2.641 | 1.068 |
| 4 | 2.02 | 26.311 | 23.095 | 3.217 | 0.576 |
| 5 | 2.12 | 25.347 | 21.873 | 3.474 | 0.257 |
| 6 | 2.19 | 25.194 | 21.534 | 3.660 | 0.186 |
| 7 | 2.22 | 25.057 | 21.316 | 3.741 | 0.081 |
| 8 | 2.25 | 25.101 | 21.278 | 3.823 | 0.082 |
| 9 | 2.27 | 25.256 | 21.378 | 3.878 | 0.055 |
| 10 | 2.30 | 25.289 | 21.327 | 3.962 | 0.084 |




(**a**) Accumulated energy absorption (**b**) Energy absorbed during each impact

**Figure 17.** Energy absorbed due to local indentation vs. impact number.

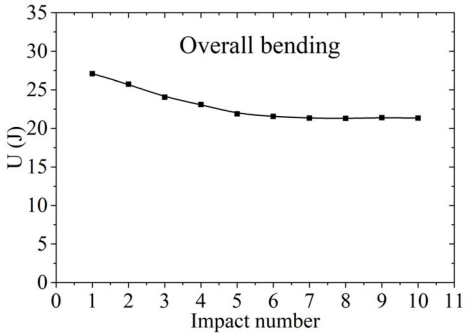



**Figure 18.** Energy absorbed due to overall bending vs. impact number.

As the number of impacts increased, the energy absorbed due to local indentation during each impact ($\Delta U_i$) initially increased and then decreased, as illustrated in Figure 17a. When the impact number reached 7, $\Delta U_i$ began to decrease as a result of the metal foam core reaching the densification stage. At this moment, the energy was mainly consumed via overall bending; subsequently, local indentation no longer increased. Correspondingly, as shown in Figure 18, the energy absorbed due to global bending under each impact decreased with the number of impacts, and the rate of change in energy absorption decreased. However, when the number of impacts was more than 7, the energy absorbed due to global bending remained almost constant.

## 4. Conclusions

In this study, the dynamic behaviors of AFSBs under repeated impacts were investigated and the mechanism of deformation and damage accumulation was examined. The relationship between the dynamic responses of AFSBs and the number of impacts was

determined, and the rebound characteristics of AFSBs and the energy absorbed due to local indentation and global bending were discussed. The following conclusions can be drawn:

(1) When an AFSB was subjected to a wedge mass impact, plastic hinges occurred at the middle span and two end supports, and the deformation of the AFSB was almost linearly distributed. The front face sheet experienced global bending accompanied by local indentation, while the back face sheet mainly displayed global bending. The failure of the front face sheet was dominated by fracture at the boundary due to axial stretching. For the metal foam core, cracks were first generated at the middle span, and then at the clamped boundaries; this led to tensile fracture. As the number of impacts increased, the deformation and damage accumulated, and the face sheets and the metal foam core exhibited progressive failure.

(2) The peak impact force, the deflection of the face sheets, and the rebound velocity increased gradually with an increase in the number of impacts, while the increments declined. However, when cracks occurred on the metal foam core and face sheets, the carrying capacity of the AFSB decreased suddenly. In this situation, as the number of impacts increased, the peak force and the rebound velocity decreased, while the deflections of the front and back faces increased exponentially.

(3) When the AFSB was subjected to external loadings, the initial kinetic energy of the impactor was mainly transformed into elastic and plastic deformation energy. As the number of impacts increased, the elastic energy of the AFSB increased but the plastic deformation energy declined. However, when the metal foam core cracked, the elastic energy that was stored by the AFSB decreased with the increase in the number of impacts, while the plastic deformation energy increased.

(4) As the number of impacts increased, the local indentation gradually increased. In addition, the energy absorbed by local indentation first increased, and then decreased. In other words, since local indentation mainly occurred during the first few impacts, when the number of impacts exceeded a specific value, the AFSB mainly experienced global bending, resulting in the energy absorption gradient of the local indentation decreasing.

**Author Contributions:** Conceptualization, K.G.; methodology, K.G.; formal analysis and investigation, M.M. and S.Z.; writing—original draft preparation, M.M.; writing—review and editing, K.G. All authors have read and agreed to the published version of the manuscript.

**Funding:** This research was financially supported by a project of the National Natural Science Foundation of China (Grant number: 12202328), and a project of the Key Laboratory of Impact and Safety Engineering (Ningbo University), Ministry of Education (Grant number: CJ202203).

**Data Availability Statement:** Not applicable.

**Acknowledgments:** The authors gratefully acknowledge the financial support from the project of the National Natural Science Foundation of China, and the project of Key Laboratory of Impact and Safety Engineering (Ningbo University), Ministry of Education.

**Conflicts of Interest:** The authors declare no conflict of interest.

## References

1. Zhu, L. Dynamic Inelastic Behaviour of Ship Plates in Collision. Ph.D. Thesis, University of Glasgow, Scotland, UK, 1990.
2. Zhu, L.; Faulkner, D. Damage estimate for plating of ships and platforms under repeated impacts. *Mar. Struct.* **1996**, *9*, 697–720. [CrossRef]
3. Zhu, L.; Shi, S.; Jones, N. Dynamic response of stiffened plates under repeated impacts. *Int. J. Impact Eng.* **2018**, *117*, 113–122. [CrossRef]
4. He, X.; Soares, C.G. Experimental study on the dynamic behavior of beams under repeated impacts. *Int. J. Impact Eng.* **2021**, *147*, 103724. [CrossRef]
5. He, X.; Soares, C.G. Numerical study on the pseudo-shakedown of beams under repeated impacts. *Ocean Eng.* **2021**, *242*, 110137. [CrossRef]
6. He, X.; Garbatov, Y.; Soares, C.G. Analysis of pseudo-shakedown of rectangular plates under repeated impacts. *Ocean Eng.* **2022**, *265*, 112609. [CrossRef]

7. He, X.; Garbatov, Y.; Soares, C.G. Pseudo-shakedown of rectangular plates under repeated impacts. *Mar. Struct.* **2022**, *85*, 103258. [CrossRef]
8. Truong, D.D.; Cho, S.R.; Huynh, V.V.; Dang, X.P.; Duong, H.D. A study on dynamic response of steel plates under repeated impacts. In Proceedings of the International Conference on Advanced Mechanical Engineering, Automation, and Sustainable Development 2021 (AMAS2021), Ha Long, Vietnam, 4–7 November 2021; Springer: Berlin/Heidelberg, Germany, 2022.
9. Banhart, J. Manufacture, characterization and application of cellular metals and metal foams. *Prog. Mater. Sci.* **2001**, *46*, 559–632. [CrossRef]
10. Madgule, M.; Sreenivasa, C.G.; Borgaonkar, A.V. Aluminium metal foam production methods, properties and applications—A review. *Mater. Today Proc.* **2023**, *77*, 673–679. [CrossRef]
11. Rajak, M.K.; Mondal, D.P.; Mehta, Y. Effect of rolling on microstructure behaviour, and mechanical properties of Mg-Al-Si alloys. *Mater. Today Commun.* **2023**, *35*, 106320. [CrossRef]
12. Lichy, P.; Elbel, T.; Kroupová, I.; Radkovsky, F. Preparation and evaluation of properties of cast metallic foams with regular inner structure. *Arch. Metall. Mater.* **2017**, *62*, 1643–1646. [CrossRef]
13. Kroupová, I.; Gawronová, M.; Lichý, P. Preparation of cast metallic foams with irregular and regular inner structure. *Materials* **2021**, *14*, 6989. [CrossRef] [PubMed]
14. Kroupová, I.; Gawronová, M.; Lichý, P.; Merta, V.; Radkovský, F. Use of molding mixtures for the production of cast porous metals. *Metals* **2022**, *12*, 1134. [CrossRef]
15. Rajak, D.K.; Linul, E. Crushing Response of Composite Metallic Foams: Density and High Strain Rate Effects. *J. Alloy. Compd.* **2021**, *871*, 159614. [CrossRef]
16. Linul, E.; Pietras, D.; Sadowski, T.; Marşavina, L.; Rajak, D.; Kovacik, J. Crashworthiness performance of lightweight Composite Metallic Foams at high temperatures. *Compos. Part A Appl. Sci. Manuf.* **2021**, *149*, 106516. [CrossRef]
17. Vincenzo, C.; Gabriella, E.; Eugenio, G. Impact response of aluminium foam sandwiches for light-weight ship structures. *Metals* **2011**, *1*, 98–112.
18. Yu, Y.; Cao, Z.; Tu, G.; Mu, Y. Energy absorption of different cell structures for closed-cell foam-filled tubes subject to uniaxial compression. *Metals* **2020**, *10*, 1579. [CrossRef]
19. Wang, X.; Cao, Z.; Fu, G. Quasi-Static Three-point bending behavior of aluminium foam sandwich with CFRP face-sheets. *Metals* **2022**, *12*, 1393.
20. Liu, K.; Liu, H.; Li, Y.; Wang, Z.; Wang, J. A simplified method for evaluating the dynamic response of the metal sandwich structure under explosion load. *Metals* **2022**, *12*, 1933. [CrossRef]
21. Guo, H.Y.; Zhang, J.X. Expansion of sandwich tubes with metal foam core under axial compression. *J. Appl. Mech.* **2023**, *90*, 051008. [CrossRef]
22. Yu, J.; Wang, X.; Wei, Z.; Wang, E. Deformation and failure mechanism of dynamically loaded sandwich beams with aluminium-foam core. *Int. J. Impact Eng.* **2003**, *28*, 331–347. [CrossRef]
23. Yu, J.; Wang, E.; Li, J.; Zheng, Z. Static and low-velocity impact behavior of sandwich beams with closed-cell aluminium-foam core in three-point bending. *Int. J. Impact Eng.* **2008**, *35*, 885–894. [CrossRef]
24. Crupi, V.; Montanini, R. Aluminium foam sandwiches collapse modes under static and dynamic three-point bending. *Int. J. Impact Eng.* **2007**, *34*, 509–521. [CrossRef]
25. Jing, L.; Wang, Z.; Ning, J.; Zhao, L. The dynamic response of sandwich beams with open-cell metal foam cores. *Compos. Part B Eng.* **2011**, *42*, 1–10. [CrossRef]
26. Wang, Z.; Jing, L.; Ning, J.; Zhao, L. The structural response of clamped sandwich beams subjected to impact loading. *Compos. Struct.* **2011**, *93*, 1300–1308. [CrossRef]
27. Jing, L.; Wang, Z.; Ning, J.; Zhao, L. The mechanical response of metallic sandwich beams under foam projectile impact loading. *Lat. Am. J. Solids Struct.* **2011**, *8*, 107–120. [CrossRef]
28. Tan, Z.; Luo, H.; Long, W.; Han, X. Dynamic response of clamped sandwich beam with aluminium alloy foam core subjected to impact loading. *Compos. Part B Eng.* **2013**, *46*, 39–45. [CrossRef]
29. Jing, L.; Su, X.; Chen, D.; Yang, F.; Zhao, L. Experimental and numerical study of sandwich beams with layered-gradient foam cores under low-velocity impact. *Thin-Walled Struct.* **2019**, *135*, 227–244. [CrossRef]
30. Qin, Q.; Wang, T. Low-velocity heavy-mass impact response of slender metal foam core sandwich beam. *Compos. Struct.* **2011**, *93*, 1526–1537. [CrossRef]
31. Qin, Q.; Wang, T. Low-velocity impact response of fully clamped metal foam core sandwich beam incorporating local denting effect. *Compos. Struct.* **2013**, *96*, 346–356. [CrossRef]
32. Zhang, J.; Qin, Q.; Xiang, C.; Wang, T. Dynamic response of slender multilayer sandwich beams with metal foam cores subjected to low-velocity impact. *Compos. Struct.* **2016**, *153*, 614–623. [CrossRef]
33. Zhou, X.F.; Jing, L. Large deflection response of sandwich beams with layered-gradient foam cores subjected to low-velocity impact. *Int. J. Impact Eng.* **2023**, *172*, 104429. [CrossRef]
34. Zhu, L.; Guo, K.; Yu, T.X.; Li, Y.G. Dynamic responses of metal foam sandwich beams to repeated impacts. *Explos. Shock Waves* **2021**, *41*, 073101.
35. Zeng, Y.; Liu, J.X.; Zhao, Y.J. Experimental research on the repeated impacts behavior of aluminium corrugated-core sandwich structures. *Shock Vib.* **2022**, *2022*, 4644029.

36. Boström, P. Collapse modes of a rigid-plastic beam on a rigid-plastic foundation. *Int. J. Mech. Sci.* **1975**, *17*, 73–84. [CrossRef]
37. Qin, Q.; Wang, T. Plastic analysis of metal foam core sandwich beam transversely loaded by a flat punch: Combined local denting and overall deformation. *J. Appl. Mech.* **2012**, *79*, 041010. [CrossRef]

**Disclaimer/Publisher's Note:** The statements, opinions and data contained in all publications are solely those of the individual author(s) and contributor(s) and not of MDPI and/or the editor(s). MDPI and/or the editor(s) disclaim responsibility for any injury to people or property resulting from any ideas, methods, instructions or products referred to in the content.